TEMPORAL CONTROL OF ENCAPSULANT RELEASE FROM NANOPARTICLE LOADED POLYMERSOMES VIA SINGLE PULSE IRRADIATION

By

GINA MARIE DISALVO

A thesis submitted to the

Graduate School-Camden

Rutgers, The State University of New Jersey

In partial fulfillment of the requirements

For the degree of Master of Science

Graduate Program in Chemistry

Written under the direction of

Dr. Grace Brannigan

And approved by

_____

Dr. Grace Brannigan

_____	_____
Dr. Julianne C. Griepenburg	Dr. Sean O'Malley
_____	_____
Dr. George Kumi	Dr. Georgia Arbuckle-Keil

Camden, New Jersey

May 2018

THESIS ABSTRACT

Temporal Control of Encapsulant Release from Nanoparticle Loaded Polymersomes via Single Pulse Irradiation

by GINA MARIE DISALVO

Thesis Director:

Dr. Grace Brannigan

Polymersomes are spherical vesicles that self-assemble from amphiphilic diblock copolymers. Their structure is comprised of a bilayer membrane and an aqueous lumen which have the ability to encapsulate hydrophobic and hydrophilic molecules, respectively. Polymersomes have received significant attention for applications in drug delivery due to their ability to control the time and location of drug release within the body; this is highly desirable in that potential side effects associated with non-specific cytotoxic drugs can be minimized. While a variety of different stimuli to initiate cargo release have been investigated, light is a particularly attractive trigger because it can be minimally damaging yet deeply penetrating at certain wavelengths and intensities. In order to reduce the dosage of light required to initiate membrane disruption, photosensitizers must be incorporated into the system. In this work, hydrophobic gold nanoparticles (AuNPs) are incorporated into the membrane of PBD_{35}-b-PEG_{20} (polybutadiene(1,2 addition)-*b*-ethyleneoxide) polymersomes. Photosensitization is brought about by the strong optical absorption associated with the plasmonic nature of the particles and the accompanying photo- and thermal-

mechanical phenomena produced upon excitation. Both nanosecond and femtosecond pulsed laser sources, tuned to a wavelength congruent with the localized surface plasmon resonance (SPR) of the incorporated AuNPs, were used to trigger encapsulant release. Herein, the interaction of single pulse laser irradiation on an individual polymersome basis has been explored. Incorporation of AuNPs in the membrane are shown to significantly reduce the rupture threshold energy for both pulse widths when compared to empty membranes. Additionally, irradiation with sub-threshold energies resulted in the formation of membrane pores with encapsulant release occurring over a time frame of two minutes. An analytical model for drug release from circular membrane pores was used to determine effective pore radii in the irradiated vesicles. Preliminary work to scale down the system to the nanoscale for use as a drug delivery system *in vivo* is also shown. This fundamental study demonstrates the ability to control encapsulant release from photosensitive polymersomes in a highly spatial and temporal manner.

Acknowledgements

I would like to take the time to show my appreciation to all that have helped me along the way. Foremost, my mentors Dr. Julianne Griepenburg and Dr. Sean O'Malley have been there to help me since my first day in this lab group. Without their knowledge, expertise and ideas I would not have been successful. A special thank you goes to Dr. Grace Brannigan for kindly agreeing to serve as my Thesis Director. I would like to thank my committee members, Dr. George Kumi, and Dr. Georgia Arbuckle-Keil, for their guidance and service on my committee. I am also very appreciative of my Graduate Director, Dr. Hao Zhu, for all the guidance that he has given me. Additionally, I would like to thank Ms. Mary Craig who has helped me every step of the way throughout my journey at Rutgers.

My lab group members also deserve a shoutout, Abby, Tyler, Cory, Ryma, Dmitriy, Anna, Asa, whether we were brainstorming or just hanging out to pass the time between classes, it was always time well spent.

I could not have done this without the support from my family and friends. I can never repay you for the motivation and inspiration you have each provided, in your own special way. My Dad and Mom whom are always supportive and let me beat to my own drum. My sisters for always being there when I need them, no matter what. Joe for loving me unconditionally and adventurously. My best friends, Shannon and Lauren, who are also formidable mothers and know the struggle like no one else does. And to all of my friends that I have met along the way on my curvy path to the finish line, you have all helped to shape me.

Dedication

This thesis is dedicated to my daughter, Katrina Marie. You are the reason I wanted to better myself and come back to school. Always remember there is nothing or nobody that can hold you back from your dreams, except you. I love you to the tooth fairy!

Table of Contents

List of Illustrations

Chapter 1

Introduction

Bilayer Vesicles

Vesicles, in biology, are tiny compartments within the body. When the vesicles are lipid-based, they are called liposomes, and self-assemble from natural phospholipids into a bilayer forming a spherical vesicle that encases an aqueous core. Self-assembly is governed by amphiphilic interactions of the polar heads and nonpolar tails thus the generation of a spherical vesicle in an aqueous environment represents an energetically favorable system.

Polymersomes (psomes), the synthetic variants of liposomes, self-assemble from diblock copolymers that mimic lipid amphiphilicity as shown in Figure 1. Two distinct compartments are created upon self-assembly: a hydrophilic core, and a membrane, comprised of a hydrophobic center. Cargo of similar hydrophilicity can be loaded into either compartment (Figure 2).

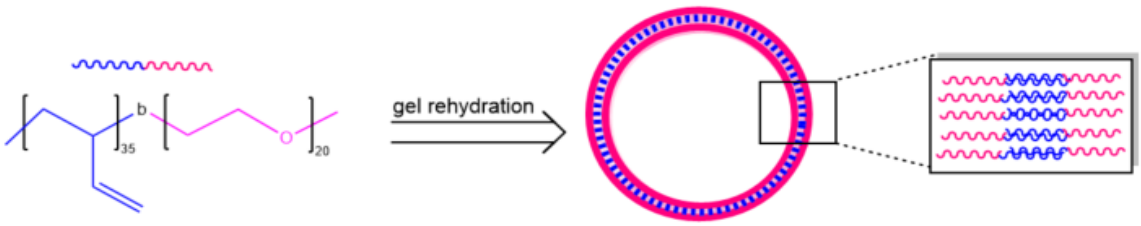

Figure 1. Schematic of polymersome self-assembly.
Structure of diblock copolymer poly(butadiene(1,2 addition)-b-ethylene oxide) which self-assembles into a spherical vesicle with hydrophobic (polybutadiene, blue) and hydrophilic (polyethylene oxide, pink) regions.

There are several major advantages for using synthetically made vesicles as drug carriers over naturally occurring liposomes. For example, membrane thickness can be increased to values >10 nm by increasing the molecular weight of the hydrophobic block.[1,2] This represents a significantly thicker membrane than that found in liposomes, which average 1-2 nm, and results in more robust vesicles with the ability to compartmentalize larger hydrophobic compounds without compromising integrity.[1]

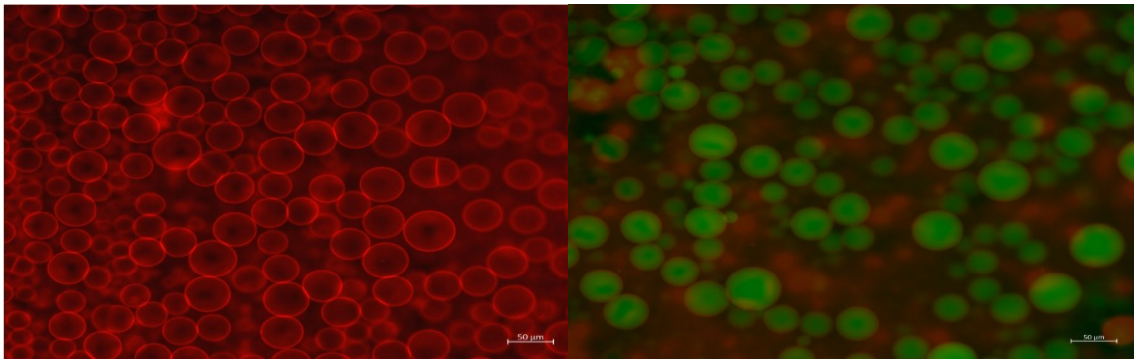

Figure 2. Fluorescent images of micron-sized polymersomes.
Two distinct compartments are shown. (Left) Nile red encapsulated in the hydrophobic region of the membrane. (Right) FITC-dextran encapsulated in the hydrophilic region of the membrane. Scale bar 50 μm.

The wide variety of block copolymers available gives rise to tunability of vesicles in terms of membrane thickness, overall size, and functionalization.[3,4] The work herein utilizes polybutadiene(1,2 addition)-*b*-ethyleneoxide (PBD_{35}-*b*-PEG_{20}) due to its robust nature and stability over large temperature and pH ranges.[5] Additionally, poly(ethylene glycol) is already approved by the FDA for use *in vivo*, making the transition from this fundamental study to potential biological applications feasible.[6]

Polymersome Delivery Systems

Targeted delivery systems are used to transport cargo to a desired location. Cargo types vary broadly and include reporter molecules, nucleic acids, chemotherapeutics and enzymes, to name a few.[7-10] Cargo transport in a carrier system is desired to subvert unwanted, off target effects; or is simply required due to the encapsulant being unable to reach the target location on its own. Once inside of the carrier, the cargo must not interact with the outside environment until warranted.

Systems with high spatiotemporal resolution release their cargo at a specific time and place in response to a stimulus. High resolution offers benefits such as controlled release, the ability to use high concentrations while reducing overall toxicity, and the minimization of off target effects.[10] Stimuli can be internal, in the carrier's local environment, such as change in pH, temperature, or redox potential.[11-13] Many efforts have also been made in the area of external stimuli, i.e. release brought about from stimuli originating from outside of the carrier's local environment; examples include ultrasound waves, magnetic fields or light.[14-16] Regardless of the specific stimulus, a controllable release mechanism that provides high spatial and temporal resolution is an essential characteristic of a controllable delivery system.

Light as the Stimulus

Light is a particularly attractive triggering mechanism because it can be highly controlled in a spatiotemporal manner. The wavelength of light required to induce change can be tuned depending on the photosensitizer that is incorporated into the system. Wavelength is a critical parameter because chromophores that exist in

biological tissues (i.e. heme, carotene and bilirubin) are highly absorbing below 600 nm.[17,18] Ultraviolet (UV) light, below 400 nm, has enough energy to cleave the chemical bonds comprising these absorbers, and lead to permanent damage to biological tissues. Wavelengths in the visible region between 400-600 nm are less energetic, resulting in less damage than UV, but some major biological molecules still have appreciable absorption in this range that decreases potential absorption depth.[19] Wavelengths between 600-950 nm, also known as the biological window, provides minimal chromophore damage and optimal tissue penetration.[20] Unfortunately, not many photosensitizers responsive to visible and near-infrared (NIR) light have been identified. For this reason, many examples in the literature utilize UV light to initiate release.

Wang et. al created light sensitive polymersomes using poly(ethylene oxide)-*b*-PSPA diblock copolymers, where SPA is a hydrophobic, spiropyran(SP)-based monomer containing a unique carbamate linkage.[21] Upon irradiation with sub 420 nm light, this moiety is isomerized into a zwitterionic merocyanine state. The transition is accompanied by a switch in membrane polarity from nonpermeable to permeable for species below a critical molar mass. This example uses continuous wave UV irradiation for twenty minutes under dark conditions. While it is well known that UV irradiation is not an ideal external stimulus due to its harmful effects to mammalian cells, this example demonstrates the ability to selectively release cargo at a specific time and place using light.

Robbins et. al and Griepenburg et. al incorporated a meso-to-meso ethyne-bridged bis[(porphinato)zinc] (PZn_2) chromophore at high concentrations into the membrane to form micron- and nano-sized polymersomes, respectively, responsive to visible light.[22,23] Confocal laser scanning was used to deliver continuous wave irradiation at 488, 543 and 633 nm for over five minutes. These wavelengths coincide to the three maxima absorption peaks found in the UV-Vis spectrum of PZn_2. While the exact mechanism was not determined, it was proposed that irradiation resulted in porphyrin energy dissipation as heat, which induced irreversible membrane changes with time. This resulted in cargo release from the vesicle. While one of the wavelengths used here pushes into the biological window, continuous irradiation of a vesicle for over five minutes is not practical *in vivo* because immobilization over such a time period is not always feasible.

Another notable example by Amstad et. al loaded psomes with AuNPs in the hydrophobic membrane.[24] Vesicles were synthesized using PEG-*b*-poly(lactic acid) (PLA) with the addition of poly(N-isopropylacrylamide) (PNIPAM)-*b*-poly(lactic-co-glycolic acid) (PLGA) and AuNPs to render them thermoresponsive and photoresponsive, respectively. Irradiation with 488, 532 and 633 nm continuous wave light for 25 minutes initiated membrane degradation and encapsulant release. AuNPs are shown to be photosensitizers for this system by selectively destroying psomes containing AuNPs while psomes without AuNPs are unaffected. Disruption of the membrane was attributed to local heating that induced amphiphilicity changes, causing holes in the membrane, eventually leading to complete degradation of the vesicle. However, the use of a thermoresponsive polymer limits the selection of

diblock copolymers and confines experimental conditions to below 40˚C, which is a major drawback of this system. Additionally, achieving rupture required irradiation times of 25 minutes.

The systems described above demonstrate the ability to selectively open psomes using a light induced mechanism. However, no examples exist using single pulse irradiation of AuNP loaded polymersomes to date. Using single pulse irradiation provides a promising method to increase spatiotemporal control as well as to investigate the laser-nanoparticle and nanoparticle-membrane interactions on a single vesicle level. The fundamental study presented herein aims to address issues associated with current systems in order to be biologically applicable in the future. Primarily, the use of continuous, ultraviolet radiation is far too damaging to be used *in vivo* and the use of block copolymers that are not biologically inert limit the application of the system.

Gold Nanoparticles Interaction with Light

In order to achieve high spatial and temporal resolution, while not causing damage to body tissues, agents with large optical cross sections that primarily relax through thermal pathways should be incorporated. Plasmonic nanoparticles certainly meet these requirements. With hydrophobic functionalization, nanoparticles can be directed toward the membrane while hydrophilic, or uncoated particles, will be directed to the aqueous core. To reduce irradiation dosage time and introduce wavelength specificity, plasmonic nanoparticles excited by single pulse laser irradiation represent an ideal combination.

Notably, noble metal nanoparticles absorb strongly in the visible to near-infrared region of the electromagnetic spectrum through a collective oscillation of the free electrons. This phenomenon is referred to as localized surface plasmon resonance (SPR).[25] The intensity and position of this peak is strongly dependent on the composition, size, shape and functionalization of the nanoparticles.[26] Thus, noble metal nanoparticles can have their peak absorption tuned from approximately 400 nm to 800 nm.

When a laser pulse is in resonance with the localized SPR of a nanoparticle, the nanoparticle becomes plasmonically excited and can result in a temperature increase of the surrounding environment.[27] Furthermore, in a liquid environment, an expanding vapor bubble around the particle can be generated and propagation of shockwaves are possible outcomes.[28] Upon irradiation, the electrons of the plasmonically excited nanoparticle undergo a sequence of relaxation processes that ultimately result in the release of thermal energy into its surroundings. The relaxation sequence follows as such: electron-electron (<500fs), electron-phonon (~1ps), and phonon-phonon (~100 ps).[29] Consequently, the laser pulse duration and local environment of the nanoparticle will heavily affect the outcome produced by excitation. Laser-particle-membrane interactions have not been addressed in detail in prior studies. This work intends to explore the fundamental principles governing these interactions.

Chapter 2

Identifying the Pulse Energy Required to Rupture Polymersomes

Introduction

The mechanisms resulting in membrane disruption will certainly depend upon the pulse energy applied to the AuNP:polymersome system. Previous works to date have only studied continuous wave irradiation and most address thermal pathways of degradation due to the use of thermosensitive polymers, even in the presence of nanoparticles. Here, single pulsed lasers are used to deliver light, in resonance (i.e. 532 nm) with gold nanoparticles embedded in the hydrophobic membrane, on a single polymersome basis.

Two different laser pulse durations are used in this study: short pulse duration and ultrashort pulse duration; i.e. nanosecond (ns) and femtosecond (fs), respectively.[30] These regimes differ in the time available for the incident light to interact with the sample. With longer pulse durations, thermal energy begins to propagate away from the nanoparticle before the pulse is over. On the contrary, ultrashort pulse durations deliver energy in a much quicker time frame resulting in thermalization processes that take place after the laser pulse is gone. This difference will significantly affect the fate of the irradiated nanoparticle-loaded polymersomes in this study.

Methods and Materials

Polymersome Preparation

Polymersomes were synthesized via the gel-assisted rehydration method.[31] Agarose films were made by spreading 1% w/v standard agarose (IBI Scientific, IA) using a 5 inch, 12g needle on a 25x 50 x .13-.17 mm glass coverslip (Electron Microscopy Sciences) and fully evaporated at 37˚C. Amphiphilic poly(butadiene-b-ethylene oxide) copolymer, PBD_{35}-b-PEO_{20} (Polymer Source, Quebec, Canada) is dissolved in chloroform (Sigma Aldrich, MO) at a concentration of 5 mg/ml. To yield fluorescent vesicles for visualization purposes, Nile Red (Santa Crus Biotechnology, CA) is added to give a final concentration of 0.5 mol%. Hydrophobic AuNPS may be added at this time for "w/ AuNPs" samples, in which the dodecanethiol-coated 3-5 nm spherical AuNPs (Alfa Aesar, Haverhill, MA) are added in a volumetric ratio of 6:1, polymer:nanoparticles. This solution of polymer, nanoparticles and fluorophore is then spread atop of the agarose film, and the solvent is removed under vacuum. A custom-made, 3D printed mold is used to generate a polydimethylsiloxane (PDMS) well, shown in Figure 3. The well is adhered to the coverslip and the Psomes self-assemble upon rehydration with 280 mM sucrose for 50 min at 45˚C. Dual-encapsulated vesicles containing a second fluorophore in the core are achieved by adding 3-5k molecular weight fluorescein isothiocyanate-dextran (FITC-dextran) (Sigma Aldrich, MO) to the sucrose rehydration buffer to a final concentration of 0.5 mg/mL.

Figure 3. PDMS well.
Rehydration well was formed using a custom-made, 3D printed mold.

Irradiation and Imaging

Vesicles remain immobilized on the agarose films for irradiation and imaging studies. Simultaneous irradiation and imaging is made feasible by a unique system that integrates an upright Zeiss optical microscope with a femtosecond (100 fs) or nanosecond (8 ns) laser systems. The Ti:Sapphire femtosecond laser system (Spectra Physics) pumps an optical parameter amplifier along with a set of harmonic crystals that allows for the output to be tuned to 532 nm. The Nd:YAG (neodymium-doped yttrium aluminum garnet; Nd:$Y_3Al_5O_{12}$) emits 1064 nm which can be tuned to 532 nm using a second harmonic crystal. The pulses from these lasers are steered through a Galilean telescope and then into the microscope and made collinear with the optical path utilizing an appropriate dichroic mirror that reflects the chosen excitation wavelength (Figure 4, left). Utilization of a dipping objective (Zeiss W N-Achroplan 20 x /0.5) allows for polymersome studies to be conducted in their native aqueous environments (Figure 4, right). The telescope was adjusted to achieve the smallest

burn spot.* Additional information regarding laser operation and safety can be found in Appendix II.

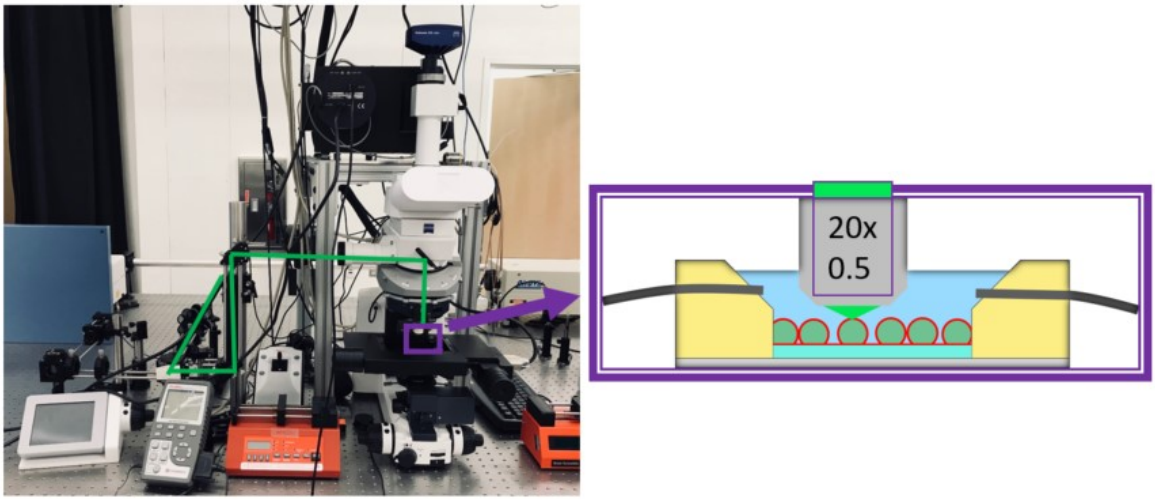

Figure 4. Microscope-Laser Setup
(Left)Image of the Zeiss AxioExaminer microscope where the green line indicates the beam path from the laser to the sample. (Right) The purple box depicts a closer look at the orientation of the dipping objective and sample.

Results and Discussion

A. Rupture Threshold

Initial studies sought to determine whether nanoparticle incorporation resulted in a reduction of the pulse energy required to induce complete rupture. Identical batches of micron-sized polymersomes were produced, differing only in their incorporation of AuNPs in the membrane i.e. with (w/ AuNP) and without (w/o AuNP). These batches contained fluorescent dyes: Nile Red and FITC-dextran in the

* Due to the difficulty in comparing burn spots between the two laser systems used in this study, it was deemed appropriate to report results in terms of pulse energy instead of fluence.

membrane and core, respectively. The average radii of these vesicles was 22.6 ± 3.4 μm, as reported in Table 2 (Appendix III).

An example of a completely ruptured vesicle upon single pulse irradiation is shown in Figure 5. As depicted, only the targeted vesicle was affected, and the surrounding vesicles remain unchanged and intact.

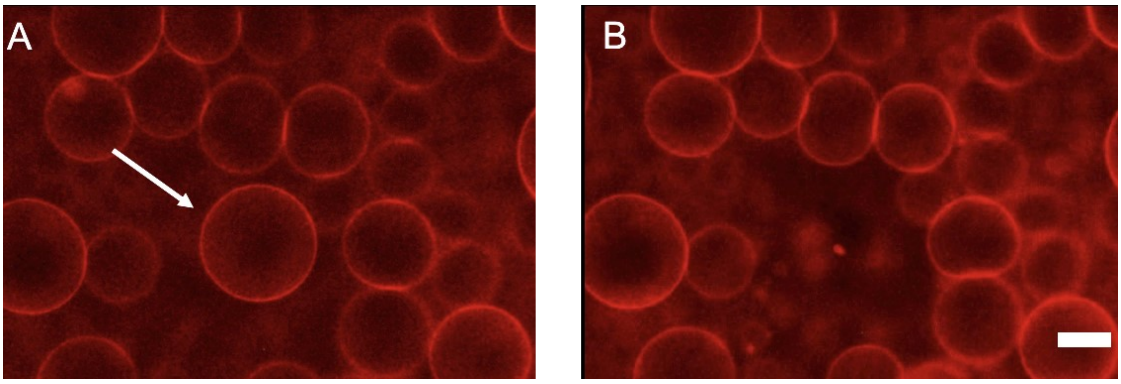

Figure 5. Polymersome rupture in response to single-pulse irradiation. Polymersome (A) before and (B) after rupture upon a single 532 nm femtosecond pulse. Nile red is encapsulated in the membrane. The white arrow indicates the vesicle that was irradiated. The scale bar represents 20 μm.

Rupture statistics for the irradiation of single vesicles by single, 532 nm, nanosecond pulses are shown in Figure 6. The pulse energy and corresponding fate of the vesicles was recorded for no fewer than 20 similarly sized vesicles. While smaller energy steps and more irradiated polymersomes would have been preferable to increase the accuracy of the study, these efforts represent a best-case scenario given the size and proximity (i.e. not touching more than one other vesicle) criteria and the available pulse energies accessible with the attenuation system. This placed a limit on the number of polymersomes available for irradiation in each sample. An

additional source of fluctuation between replicates that is difficult to control, could be attributed to nanoparticle concentration localized at the point of irradiation.

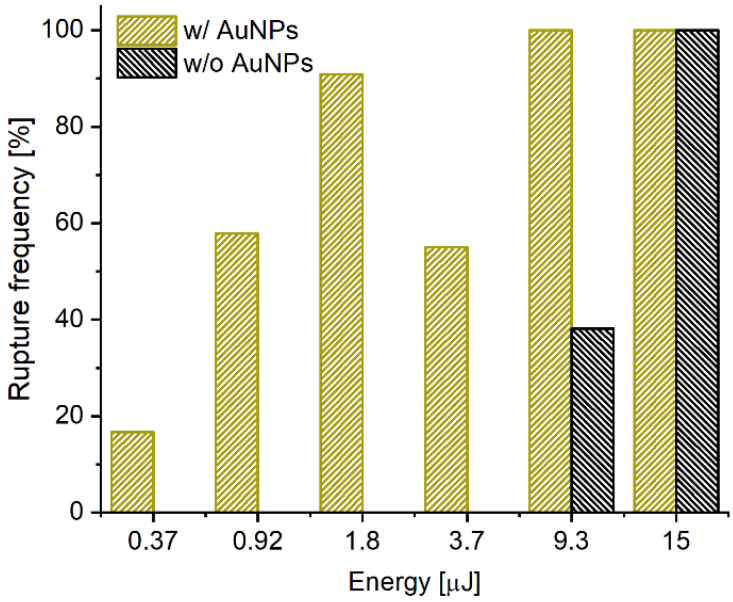

Figure 6. Rupture statistics for polymersomes using nanosecond irradiation. Rupture frequency of polymersomes with AuNPs within the membrane (gold) and without AuNPs (black) are shown. These percentages represent the complete rupture upon irradiation by a single 532 nm pulse of nanosecond pulsed irradiation at the specified energies.

Vesicles w/o AuNPs experienced a rupture rate of 100% at 15 μJ, which decreased to 39% when the pulse energy decreased to 9.3 μJ, and by 3.7 μJ, rupture was no longer observed. Vesicles w/ AuNPs in the membrane show a distinct reduction in energy to bring about rupture. Even at the lowest pulse energy of 0.37 μJ, polymersomes containing plasmonic nanoparticles still ruptured at a rate of 17%.

This represents at least a 10-fold decrease in rupture threshold† for psomes w/AuNPs. Moreover, at 9.3 μJ vesicles w/ AuNPs ruptured 100% of the time while those w/o AuNPs experienced a rate of only 38% which further indicates the enhanced photosensitivity of vesicles containing plasmonic nanoparticles in the membrane.

Figure 7 illustrates vesicle rupture rates for the femtosecond pulse durations. Statistics were gathered for this graph the same as described for Figure 6. In the femtosecond case, the initial pulse energy required to induce observable rupture for vesicles w/ AuNPs was 0.21 μJ; therefore, the rupture threshold lies in the 0.057-0.21 μJ range. The energy required to observe rupture in vesicles w/o AuNPs is 3.5x higher at 0.73 μJ. Similar to the nanosecond results, the vesicles w/ AuNP had a 100% rupture rate at this energy. Hence, for both pulse durations (ns and fs), vesicles with AuNPs present in the membrane were more sensitive to the incoming irradiation.

Femtosecond energy required to produce rupture statistics similar to nanosecond irradiation is significantly lower. The reduction in energy between fs and ns plasmonic excitation for 3 nm AuNPs can be explained, at least from a thermal standpoint, by a recent article published by Metwally et. al.[32] In this article, they

† Critical threshold values for such laser-based processes are typically extrapolated using the so called "blow-off" model $\zeta \propto \ln(E/E_{th})$ where, ζ is as measurable associated with an ablation and E_{th} is the threshold energy which is determined via regression analysis. [J. E. Andrew, P. E. Dyer, D. Foster, and P. H. Key, Appl. Phys. Lett. 43, 717 (1983)] The limited size of the rupture datasets however limit the appropriateness of such a model in this study therefore it was not used.

investigated the fluence required for the temperature immediately outside of variously-sized AuNPs to reach the spinodal temperature‡ of water which initiates

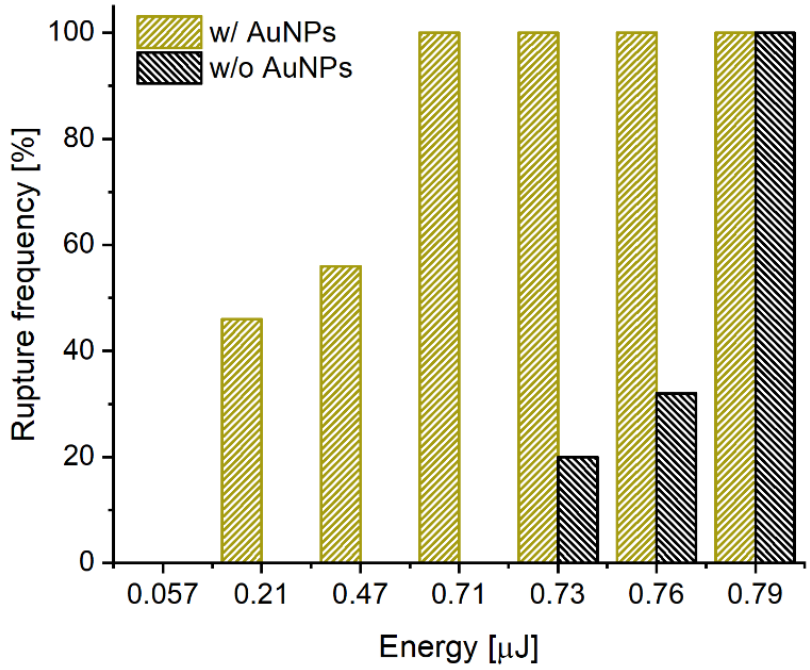

Figure 7. Rupture statistics for polymersomes upon femtosecond irradiation. Rupture frequency of polymersomes with AuNPs within the membrane (gold) and without AuNPs (black) are shown. These percentages represent the complete rupture upon irradiation by a single 532 nm pulse of femtosecond pulsed irradiation at the specified energies.

the formation of a vapor layer. This was examined for both ns and fs pulse durations at wavelength 532 nm. It was found that, for sub 20 nm AuNPs, the fluence needed to reach the spinodal temperature was significantly larger for nanosecond excitation

‡ The authors proposed that the vapor bubble formation around an excited nanoparticle coincides with the water layer immediately outside the particle reaching the spinodal temperature. Spinodal decomposition occurs at the spinodal temperature and is illustrated on phase diagrams with a miscibility gap.[33] At this point, the solution of two or more components are no longer miscible and will separate into distinct phases homogeneously throughout the material.

than with femtosecond irradiation. They propose that thermal dissipation of energy out of the particles during delivery of a ns pulse suppresses the peak temperature of the water layer. Femtosecond irradiation does not experience this thermal-dissipation during the pulse duration because all of the incident energy is delivered to the particle in a time frame less than the electron-phonon (~1 ps) and phonon-phonon (~100 ps) relaxation times.[29] Hence, the corresponding thermal energy is delivered essentially at once to the water surrounding the particle and a higher temperature can be attained for a given fluence.

Reaching the spinodal temperature of water for the nanoparticles loaded in the polymersome membrane may not be critical, given that PBD has a relatively low water permeability. Nonetheless, it is reasonable to conclude that some critical temperature exists that initiates membrane disruption such that rupture results, especially in the case of ns irradiation.

Samples w/o AuNPs were used as a control to demonstrate the photosensitizing ability of AuNPs loaded into the membrane of PBD_{35}-*b*-PEG_{20} polymersomes. The effect of pulse duration was also explored by repeating the same experiment using two durations that differ by a factor of 80,000 i.e. 100fs and 8ns. The pulse duration is shown to have a significant effect on the required pulse energy to bring about rupture.

B. FITC-dextran Encapsulation

The encapsulation of FITC-dextran into the aqueous lumen has been reported to interact with the inner leaflet, i.e. inner layer, of the polymersome membranes.[34]

We investigated the extent of the impact of this interaction on our rupture study by evaluating vesicles with and without FITC-dextran in the hydrophilic core. Just as in the previous study, giant PBD_{35}-*b*-PEG_{20} polymersomes were formed both with and without AuNPs in the hydrophobic membrane. Vesicles were singled out and irradiated by a single, femtosecond pulse in order to examine their photosensitivity.

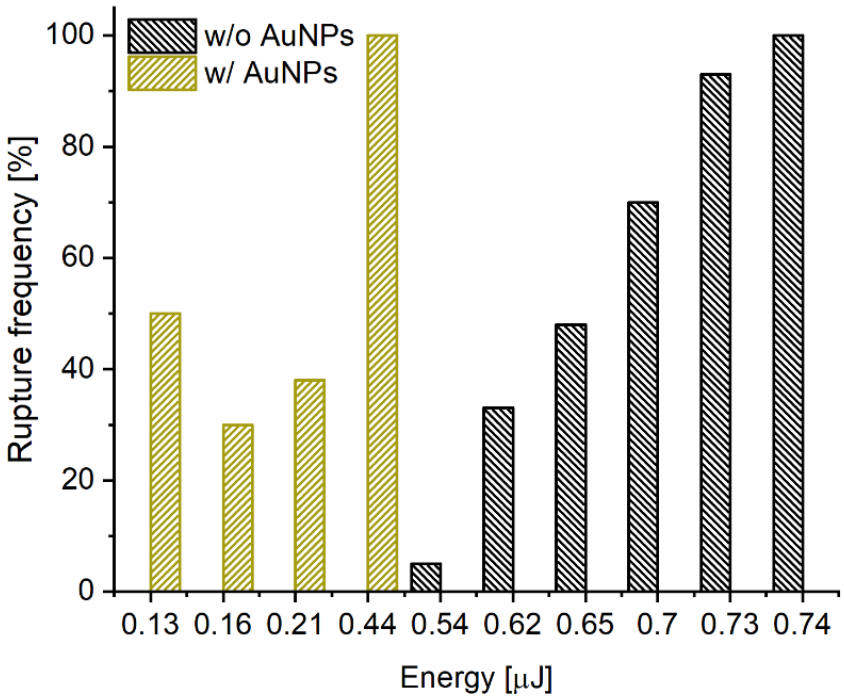

Figure 8. Rupture threshold for vesicles without FITC-dextran in the core. Each bar represents the percent of polymersomes that ruptured completely upon a single, 532 nm pulse of irradiation at the specified pulse energy from the femtosecond laser.

When juxtaposed to Figure 7, Figure 8 shows that both vesicle types are observed to rupture more readily at a lower pulse energy when they do not contain FITC-dextran in their aqueous lumen. This result of decreased photosensitivity with

dextran encapsulation is opposite to the trend found by Kamat et. al. who demonstrates an increase in photosensitivity with dextran incorporation.[34] The authors demonstrate an increase in photosensitivity and a decrease in elastic modulus, for PBD_{35}-*b*-PEG_{20} polymersomes, that scales with the dextran molecular weight. The mechanism they put forth states the dextran penetrates the hydrophilic corona and reduces interfacial tension thereby increasing the area of the inner leaflet and generating asymmetrical stress in the bilayer that destabilizes the membrane. However, this reported effect was weaker for lower Mw dextrans, such as that conjugated to the FITC dye in this study (3-5000 Da). Several important distinctions between this work and that in the Kamat study are: (1) inclusion of AuNPs in the membrane, (2) molecular weight of the dextran used and (3) laser type used for irradiation. Further investigation is needed to clarify the role played by FITC-dextran in the observed decrease in photosensitivity.

Conclusion

The addition of AuNPs into the membrane of PBD_{35}-b-PEG_{20} polymersomes decreased the rupture threshold for both ns and fs pulse durations. In the nanosecond regime, AuNPs decrease the rupture threshold by ~10x in comparison to the control. The rupture threshold for ultrashort, femtosecond pulses is reduced by ~3.5x upon the addition of AuNPs into the membrane. The greater energy required for rupture with ns vs fs pulses may be explained in part from a thermal standpoint due to the dissipation of heat away from the source during ns irradiation which thereby reduces the temperature attainable in the liquid immediately outside of the particle.

Encapsulants also affect the rupture threshold energy as seen with the investigation of the encapsulation of FITC-dextran. This small molecule increased the rupture threshold of the vesicle by 30-40%, regardless of AuNP incorporation. Further investigation is crucial to understanding the possible mechanisms responsible for this effect.

In this study, the self-assembly of photosensitized polymersomes that can be ruptured with high spatial and temporal resolution using single pulse irradiation in resonance with membrane-encapsulated AuNPs is demonstrated. The rupture threshold for such vesicles is elucidated for two pulse durations: nanosecond and femtosecond.

Chapter 3

Pore Formation and Controlled Release

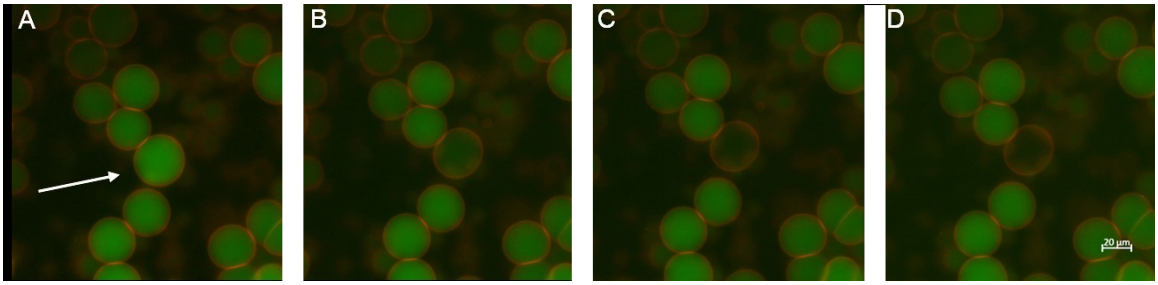

Figure 9. Vesicle poration and encapsulant release in response to lower pulse energy.
The irradiated vesicle (indicated by the white arrow) releases FITC-dextran from the core, while the Nile red in the membrane shows a generally undisrupted membrane. (A) the vesicle before irradiation with 532 nm femtosecond pulse. (B-D) shows a decrease in FITC-dextran fluorescence at 20, 80 and 120 seconds, respectively.

Introduction

A reduction in pulse energy, such that the polymersomes do not undergo rupture, can lead to pore formation in the membrane and subsequent encapsulate release. As opposed to the instantaneous release event experienced with rupture, the formation of a pore results in the release occurring over some finite timescale. At pulse energies with a low likelihood of rupture, the overall spherical shape of the vesicle can remain intact and with little to no perceivable buckling and/or distortion of the membrane. Figure 9 shows a time series of fluorescence images of such an event. Given that photosensitization, in the case of AuNP loaded vesicles, is mediated by the plasmonically excited nanoparticles it is sufficive to say that the “effective” pore may be formed from (a) an ensemble of nanosized pores over the irradiated area or (b) the close proximity where the photomechanical event is brought about by the

excited particles could act in a coordinated manner to form a single micron-sized pore.

Materials and Methods

Polymersome preparation

Polymersomes were synthesized via methods described in Chapter 2.

No additional purification steps are necessary for hydrophobic encapsulants, however, excess hydrophilic encapsulants (i.e. FITC-dextran) must be removed via exchange with fresh buffer while the vesicles are attached to the agarose film. A gentle method must be employed to prevent dislodging of the vesicles from agarose. This is achieved using two syringe pumps that use 30 mL syringes at a rate of 1ml/min. One pushes fresh buffer into the well and the other siphons the excess out of the well, as shown in Figure 4. Each syringe has a blunt tip needle with tubing attached that is fed into one end of the PDMS well.

Irradiation and Imaging

See methods, Chapter 2.

Graphical determination of Encapsulant Release using Fluorescent Intensity

In order to examine release characteristics of the porated vesicles, a series of fluorescence images were taken at regular intervals (10 s) that began ~3 s after the arrival of the incident laser pulse. The images were analyzed by selecting a region of interest (ROI) within the targeted polymersome and recording the average fluorescence intensity value. A background ROI was used to offset any excess

fluorophore and/or bleaching that may have occurred during the time series and was subtracted from the intensity of the fluorescent ROI to yield a corrected intensity which was then normalized to the pre-irradiated intensity (example calculation in Appendix III, Table 1). A minimum of 3 (non-rupturing) vesicles were measured at each pulse energy and graphed as the mean with error bars denoting the standard error of the mean (SEM).

Results and Discussion

A. Encapsulant Release

Given that a rupture frequency of ~50 % is observed for pulse energies at approximately 200 nJ (0.20 μJ) this served as the upper energy bound for the poration study. As shown in Figure 10, the fluorescence intensity, and therefore the encapsulant, decreases in an exponential manner for all energies except at the lower bound of 32 nJ where the membrane presumably reseals on a timescale equal to or shorter than the time step (i.e. 10 s) of this study. For the case of pulse energies near the upper bound (140-220 nJ), encapsulant release occurs rapidly with a large degree (~80%) of the vesicle contents escaping (Figure 11). Energies in the middle of the range (50-110 nJ) result in steady release with the removal of ~60% of the contents. Given that the fluorescence continues to diminish up to the endpoint, it can be inferred that these pores are stable (i.e. did not grow boundless, to rupture, or close) during the ~2 min timeframe. Irradiation with pulse energies at the lower bound (~30 nJ) leads to a small reduction (~13 %) in the fluorescence signal which then quickly levels-off, indicating a short-lived pore that quickly self-heals.

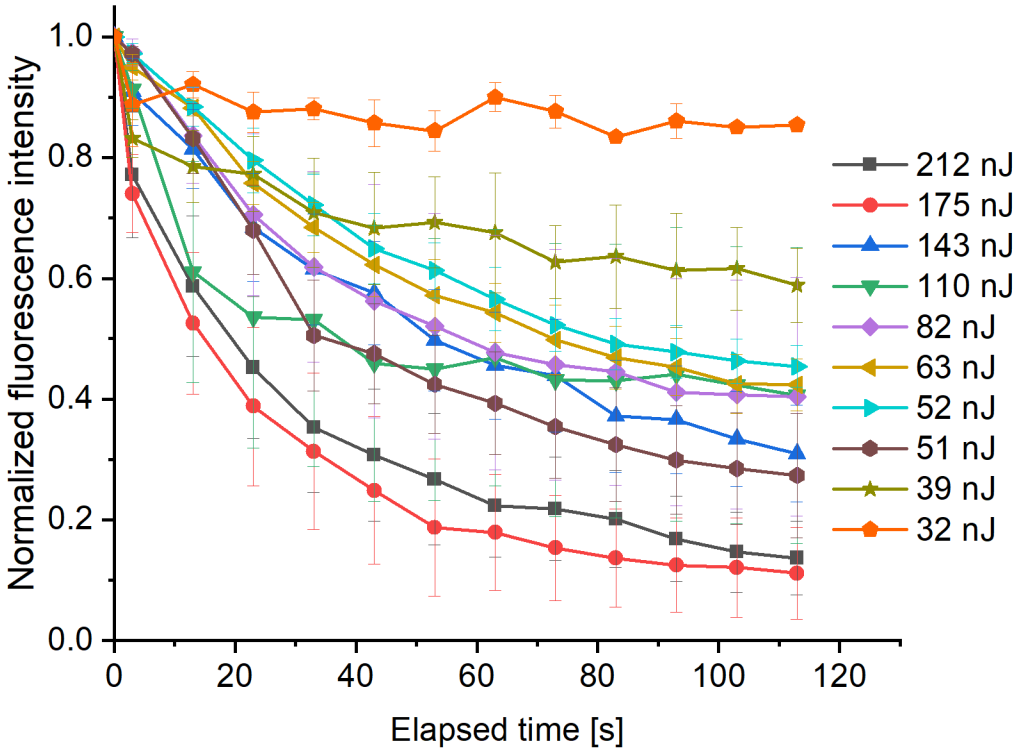

Figure 10. Release profiles of encapsulant from AuNP loaded polymersomes with varying pulse energies.

Normalized fluorescence intensity of FITC-dextran inside the core of polymersomes w/AuNPS in the membrane that were individually irradiated with a single, 532 nm pulse. Pulse energies are indicated by color in the legend on the right. Data is shown as the mean of at least 3 vesicles and error is shown as SEM.

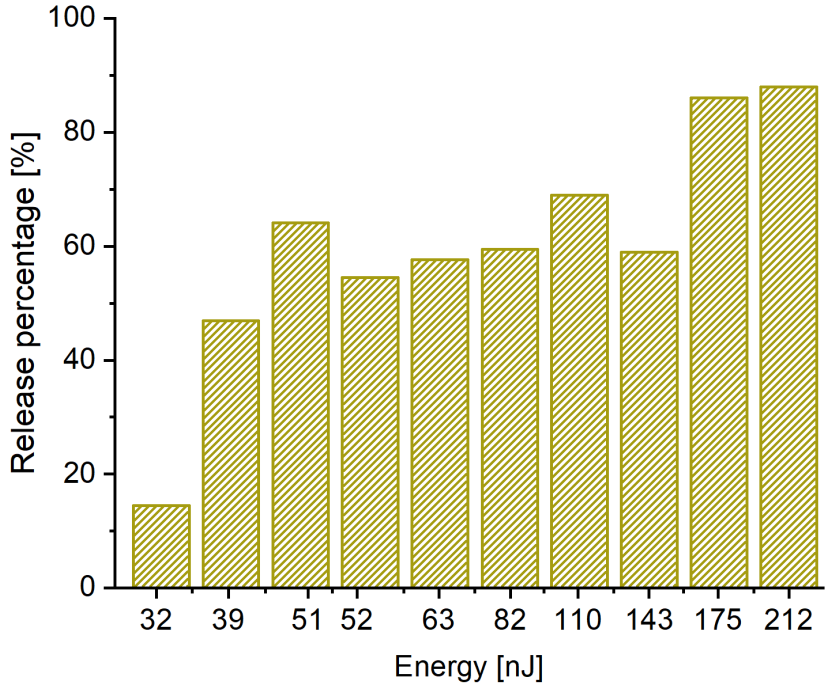

Figure 11. Percent released of total encapsulated FITC-dextran
The percentage of FITC-dextran that escaped by time point 120 seconds in Figure 10.

Additionally, a control experiment was performed to verify that AuNPs indeed photosensitized the polymersomes (Figure 12). A batch of polymersomes identical to the polymersomes evaluated in Figure 10 were assembled without the AuNPs. Poration is still observed in these empty membrane vesicles, although a much higher pulse energy is required. Exposure of polymersomes w/o AuNPs to 200nJ of 532 nm pulse resulted in <20% release of encapsulant. This specific energy shows an interesting result in the first 30 seconds that indicates some release of the encapsulant and then levels off, indicating self-healing, which was not observed for vesicles w/ AuNPs at this energy.

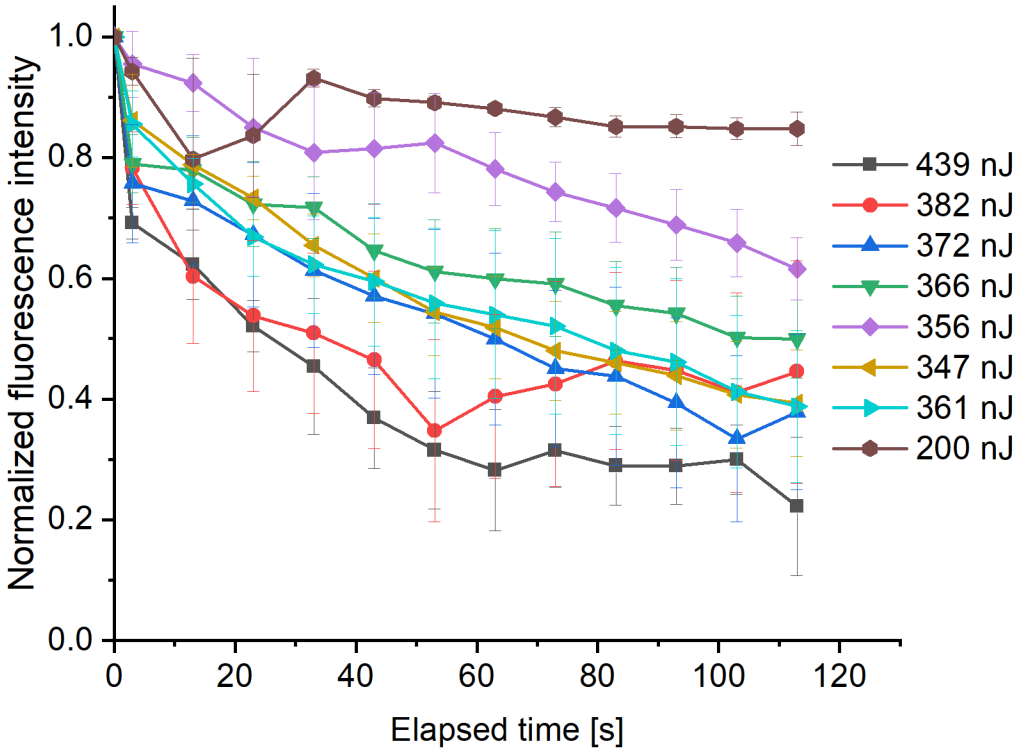

Figure 12. Release profile of encapsulant from polymersomes without AuNPs. Normalized fluorescence intensity of FITC-dextran inside the core of polymersomes w/o AuNPS that were individually irradiated with a single, 532 nm pulse. Pulse energies are indicated by color in the legend on the right. Data is shown as the mean of at least 3 vesicles and error is shown as SEM.

B. Quantification of Effective Pore Size

Determination of the pore size formed within the membrane is an area of particular interest, especially for the case of plasmonic nanoparticle-mediated poration of vesicles. Direct measurements of pore size via microscopy technique, regardless if they are electron- or optically based, would be extremely difficult; this is compounded by the delicate nature of the polymersomes, the requirement that the

irradiation occurs from above the copolymer/gel film, and the likelihood that individual pores may only be several nanometers in size and ultimately self-heal.

A recent theoretical article by Simon and Ospina provides a method to indirectly quantify effective pore size from temporal release curves.[35] As seen in Figure 9 and found by Levin et al., taking an analytical approach, the concentration of solute molecules decreases exponentially through an open pore (Equation 1).[36]

Equation 1: $$\boldsymbol{n(t) \sim e^{-\frac{t}{\tau}}}$$

Here, n is the solute concentration, t is elapsed time, and τ is a characteristic release time. Simon and Ospina derived an expression that relates the release time to the radius of small circular pore formed within a vesicle membrane through which the encapsulant escapes, see Equation 2. As illustrated in Figure 13, R is the radius of the vesicle, D is the diffusion coefficient of the solute, and θ_0 is the half-angle subtended by the pore. This expression yields the pore radius, a, when combined with the simple geometric relation for small angles.

Figure 13. Schematic representation of a spherical vesicle.
R is the radius of the sphere and a is the base radius of the cap: angle Θ_0 is the apex of the angle of the spherical cone. [Published by Simon and Ospina 2016][35]

Equation 2: $$\boldsymbol{\tau = \frac{1}{21}\frac{R^2(2\theta_0^2+35\pi^2-35\pi\theta_0)}{D\theta_0(-4\theta_0+5\pi)}} \quad ; \quad \boldsymbol{a = R\theta_0}$$

This expression was derived as a quasi-analytical approach to modeling the release of molecules through ultra-small pores where the pore size is comparable to or smaller than the mean free path of the solute molecule, i.e. an effusion process. Instead of taking an exact approach for effusion based on random walk, Simon and Ospina choose to model the system using a diffusion-based approach with the application of mixed Neumann-Dirichlet boundary conditions.[35,36] Such an approach is more appropriate for the pores formed in this study since they will most likely be significantly larger than the mean free path of the FITC-dextran.

The release time, τ, was determined by fitting each fluorescence intensity decay curve with an exponential model of the form $y(t) = Ae^{-t/\tau} + y_0$ in Origin (OriginLab Corp, 2018). A diffusion coefficient, D, of 118 μm/s was used for the FITC-dextran solute in a 10% sucrose solution as determined using the Stokes-Einstein relation. Vesicle radius, R, was measured for each porated polymersome using Zen imaging software (Zeiss Co. Mathematic) to solve for the pore size of each release curve shown in Figure 10. Values are given in Appendix III, Table 2.

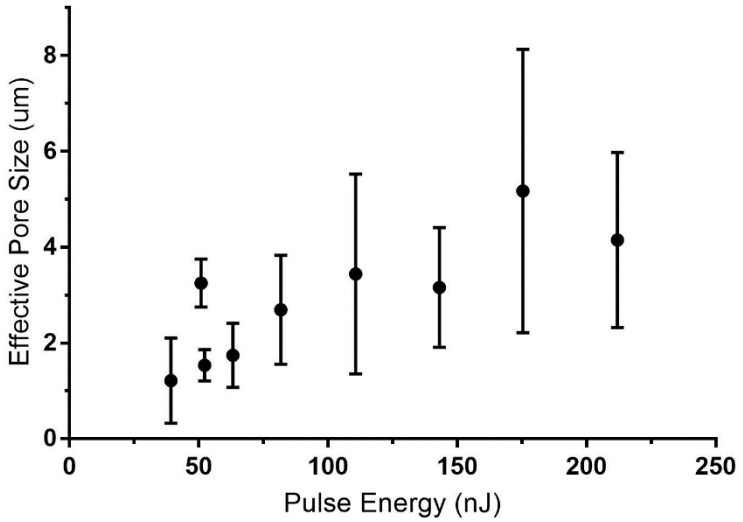

Figure 14. The effective pore radius as a function of pulse energy.
Error bars show the standard deviation of the pore size.

Figure 14 depicts the mean effective pore radius as a function of pulse energy. In general, pore size is shown to increase with pulse energy; where, the smallest and largest mean pore sizes are 1.2 μm and 5.2 μm. Note, the mean pore size at 32 nJ is omitted due to the data not being suitable for fitting (see Appendix III). At higher pulse energies, vesicle irradiation has a ~50% chance of resulting in rupture and therefore represent the upper limit for structurally stability. The largest pore radius calculated from an individual release curve was 9.5 μm and was formed in a vesicle with a 24.3 μm radius. This represents a factional pore/vesicle surface area of 0.15. Above this value, rupture will occur as the pore grows unbounded to consume the entire vesicle.

Conclusion

This novel study demonstrates the encapsulant release through pore formation created in PBD_{35}-b-PEG_{20} polymersomes as a result of single pulse irradiation. Percent release from polymersomes loaded with AuNPs ranged from 13 to 80%, on a mean-basis, where percent release increased with pulse energy. Nanoparticle photosensitization was indicated by the larger release percentage for vesicles containing AuNPs. For 200 nJ femtosecond pulses, polymersomes w/ AuNPs release approximately 80% of their encapsulant as opposed to polymersomes w/o AuNPs that only released ~20%. This represents the ability to tune the encapsulant release from vesicles while they maintain their overall structural shape.

Fluorescence intensity of the FITC-dextran encapsulant was observed to decrease exponentially with time from single pulse irradiated vesicles. At low pulse energies, a leveling off of the fluorescence signal is indicative of a self-healing pore within the two-minute time frame of this study. By applying Simon and Ospina's diffusion-based model for encapsulant release to the release curves, an effective pore radius was determined. Pore size is shown to gradually increase with increasing pulse energy but was not found to exceed 15% of the vesicle's surface area, signifying the critical value between poration and rupture.

Chapter 4

Nanovesicles

Introduction

Chapter 2 and 3 describe a polymersome-nanoparticle system self-assembled on the micron scale to facilitate single-vesicle, single-pulse studies by means of fluorescent microscopy. However, to adapt this system for practical applications in drug delivery, the system must be scaled down to the optimal size for biological drug carriers which has been shown to be between 70-200 nm in diameter.[37] A significant amount of studies have been performed on liposomes to determine the ideal balance between size, circulation time, and drug encapsulation ability, as the size of these carriers determines the overall fate of the vesicle *in vivo*.[38] While larger vesicles have greater drug storage capacities, they have relatively short circulation times due to capture by the reticuloendothelial system. Vesicles smaller than 100 nm have been shown to interact less with plasma proteins, and circulate longer in the blood due to evasion of capture by the reticuloendothelial system.[39] Long circulation times are necessary to provide adequate time for passive tumor uptake through the enhanced permeability and retention (EPR) effect.[40]

Therefore, this chapter seeks to "scale-down" the micron system to a biologically applicable size: the nanoscale. Here, psomes created on the nanoscale will be referred to as nanovesicles. Factors governing nanovesicle formation will be explored, including the volume of resuspension solvent, the relative nanoparticle concentration, the polymer concentration and different filtration techniques. While

these factors have been explored in the literature for some polymersome systems, the incorporation of nanoparticles into the hydrophobic region of the membrane during the self-assembly process of nanovesicles has not been explored. Thus, this chapter will investigate these factors so that the release dynamics of the micron- vs. nano-scale can be determined for future studies.

Materials and Methods

Nanovesicles were prepared using a solvent injection method that utilizes a 30:70 ratio of organic to aqueous phases.[41] The solvent injection method is an established technique for the preparation of large volumes of polymersomes of various size regimes. This method of formation is based on the limited solubility of each of the components of the diblock copolymer in the two solvents as well as the limited miscibility between the organic and aqueous solvents.[41] The copolymer, PBD_{35}-*b*-PEO_{20} (Polymer Source, Quebec, Canada), was dissolved in THF (Sigma Aldrich, MO) at a concentration of 1.5 mM, unless otherwise noted. To yield fluorescent vesicles, 1.0 mol % of Nile Red (Santa Cruz Biotechnology, CA) can be added to the organic solution. Next, the necessary volume of deionized distilled water (ddH_20) was added to the solution to 70% of the total volume. The mixture was then vortexed continuously for five minutes at 10k RPM to form an emulsion between the organic and aqueous phases, resulting in the spontaneous self-assembly of nanovesicles.

Dynamic Light Scattering

The hydrodynamic diameter was determined using dynamic light scattering (DLS). This is a measurement of the apparent size of the dynamic hydrated/solvated particle using the diffusional properties of the particle.[42] The DLS gives the diameter of a hypothetical, hard sphere that diffuses with the same speed as the particle under examination.[43]

A Malvern Zetasizer NanoZS was used in conjunction with Zetasizer Software (Version 7.11). The average of three measurements, with 11 runs each, was used to generate the graphs, shown in Figures 15-17, and the error bars represent standard deviation between the average size determined in each run. The material was set to polyethylene glycol (Refractive Index: 1.467, Absorption: 0.001), and the solvent was set to water at 25˚C (Refractive Index: 1.330, Viscosity: 0.8772 cP). Disposable cuvettes (DTS0012, Malvern Panalytical, USA) were used. The scattering angle was set at 173˚ backscattering. The instrument was set to seek for optimal scanning position with automatic attenuation selection.

Once raw samples ("not filtered") were analyzed for size, the samples were filtered using a 0.45 μm PTFE syringe filter (GS-TEK, USA) to remove aggregates and reanalyzed with DLS ("filtered").

Cryogenic Transmission Electron Microscopy

Two samples were sent to NanoPort Europe Thermofisher Scientific (formerly FEI, Netherlands) for cryogenic electron microscopy (cryoEM) imaging to visualize morphology and confirm loading of the hydrophobic dodecanethiol coated nanoparticles within the hydrophobic region of the bilayer membrane. CryoEM is a

preferred method of imaging for polymersomes to preserve their vesicular structure upon vitrification in liquid ethane, as opposed to drying associated with High Resolution TEM which would result in rupture. To prepare these samples for cryoEM it was necessary to rid the sample of all organic solvent. Once polymersomes are formed, their outer hydrophilic PEG brush allows for suspension in aqueous solution. Thus, solvent exchange from the THF/ddH_20 mixture used during self-assembly to pure ddH_20 was performed by removing the organic component with an Amicon Ultra 4 centrifugation filter (Sigma Aldrich, MO). Approximately half (500 µl) of the prepared sample was put into the Amicon filter along with 4 ml of ddH20. This was spun in the centrifuge at 33K RPM for 10 minutes. The filtrate was notably colorless, indicating little to no permeation of the fluorescent nanovesicles through the filter. Another 4 ml of ddH_20 was added with the rest of the prepared sample, centrifuged again, and this entire process was repeated two additional times; approximately 400 µl of sample was recovered from the filter. This process was repeated for each sample independently. Samples were packed and shipped internationally by air.

CryoEM images were generated using a Talos L120 transmission electron microscope at 120kV acceleration voltage with a Ceta camera (4kx4k) in Low Dose mode. Polymer vesicles were vitrified using the FEI Vitrobot Mk4. All images were collected with the total dose 20e/A^2s and at the pixel size 2.28 Å.

Results and Discussion

To photosensitize nanovesicles, 10 µl of 3-5 nm dodecanethiol-coated AuNPs (Alfa Aesar, Haverhill, MA), suspended in toluene, was added to the organic mixture.

Unfortunately, the AuNPs suspended in toluene created a visible phase separation which was not completely miscible within the THF. This was resolved by evaporating off the toluene and resuspending them in a miscible organic solvent, THF. Thus, the amount of rehydration solvent required to incorporate the AuNPs into the membrane was the first thing optimized. Ten microliters of 3-5 nm dodecanethiol-coated AuNPs (Alfa Aesar, Haverhill, MA) were placed into a 2.0 mL centrifuge tube and placed on a hotplate at 40˚C to fully evaporate the toluene. After allowing to cool, the nanoparticles were resuspended in 10, 20 or 40 µL of THF (Sigma Aldrich, MO).

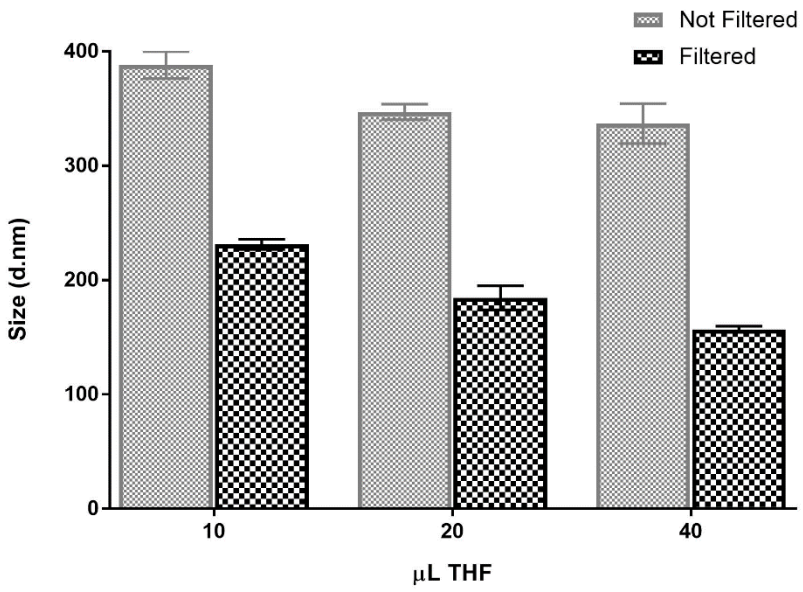

Figure 15. Hydrodynamic nanovesicles prepared with varying amounts of AuNP resuspension solvent.
The hydrodynamic diameter of nanovesicles prepared with varying amounts of AuNP resuspension solvent, determined by DLS. The blue bars represent raw prepared samples, while the red bar indicates the sample post filtration with 0.45 µm PTFE syringe filter. The smallest vesicles were observed when using 40 µL of THF to rehydrate the 10 µL of AuNPs and filtered. Error bars show standard deviation of three measurements.

Results in Figure 15 show that 40 μL of resuspension solvent resulted in the smallest, and most monodisperse vesicles after filtration. Going forward, this was the protocol used to prepare AuNPs for the solvent injection method of self-assembly.

It was also necessary to investigate if the concentration of AuNPs would affect the size and/or formation of the nanovesicles. This experiment was performed according to the protocol outlined above, however, the amount of AuNPs that were dried in the centrifuge tube was altered to include either 0, 2.5, 5, 10 and 20 μL suspended in 40 μL of THF to compare the relative concentrations of these particles. Figure 16 shows that the smallest vesicles were observed when 2.5 μL of AuNPs were dried in the tube before resuspension, however, the 20 μL sample was still in the optimal size range i.e. 70-200 nm. The protocol moving forward uses 20 μL of AuNPs to observe any morphological defects caused by maximal nanoparticle loading on cryoEM.

To fully optimize this system, different concentrations of polymer were also explored: 1.5 mM and 3.0 mM. These samples were made with the same solvent injection method; however, the final concentration of the copolymer solution was altered. These samples were then analyzed by DLS and showed no significant difference in hydrodynamic radius (Figure 17).

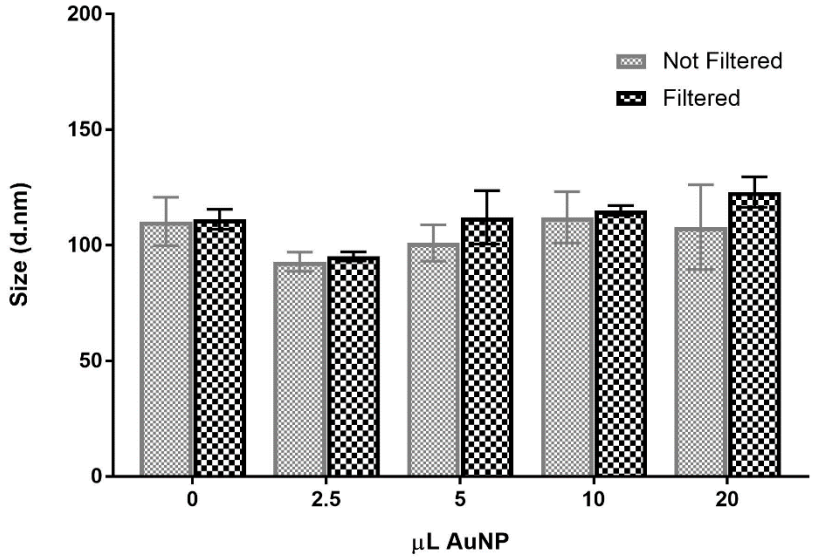

Figure 16. Hydrodynamic diameter of nanovesicles prepared with varying [AuNP]
The smallest vesicles were observed when 2.5 μL of AuNPs were rehydrated with 40 μL of THF. The addition of AuNPs results in minimal size variation. Error shown is standard deviation.

The next step in characterization of the nanovesicles was cryoEM analysis to determine morphology. Preparation of samples for cryoEM required removal of all organic solvent which was performed with Amicon filters, outlined previously in the materials and methods section. According to DLS, as shown in Figure 17, a slight swelling occurred after the solvent switch. This diameter increase was expected and is attributed to the expansion of the PEG brush on the outer membrane which is no longer compressed as a result of any confining hydrophobic regions of THF in the sample prior to the solvent switch. Overall, the DLS indicates that the solvent switch had no significant and/or detrimental effect on the size of the particles.

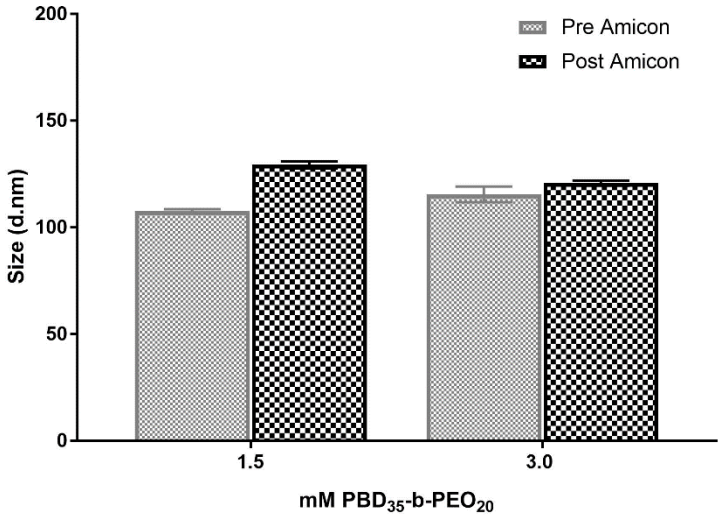

Figure 17. Hydrodynamic diameter of nanovesicles prepared with two different concentrations of diblock copolymer.
Hydrodynamic diameters are shown before and after filtering with an Amicon Ultra 4 centrifugation unit. A very slight swelling post-amicon is observed, however, no significant difference in vesicle size between the two different diblock copolymer concentrations was observed. Error bars show the standard deviation of 3 measurements.

A cryoEM image of nanovesicles prepared according to the protocol outlined in materials and methods is shown in Figure 18 (FEI, Netherlands). Unfortunately, due to shipping via air and extreme pressure changes, the nanovesicles aggregated and/or ruptured, resulting in the coalesced circular regions as shown in the image. However, it is clear from this image that the nanoparticles which were contained within the hydrophobic region of the membrane are arranged in a spherical pattern, with diameters in agreement with DLS results.

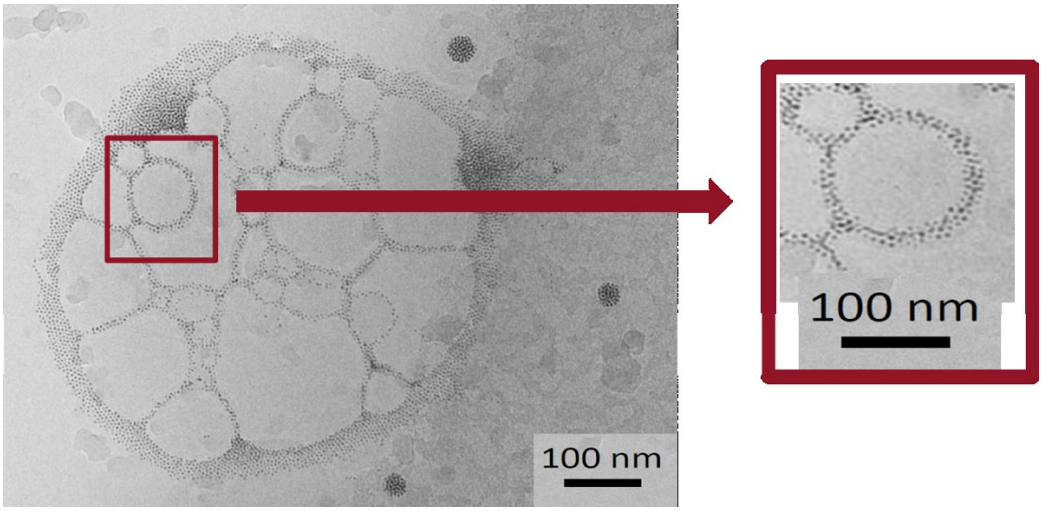

Figure 18. CryoEM images of nanovesicles (NanoPort Europe). The enlargement shows a 100 nm vesicle with 2-3 gold nanoparticles stacked in the membrane, shown as a darker contrast.

An important conclusion from this image is the location of the AuNPs, which appear in a circular pattern. This indicates that they are located exclusively in the membrane (which can be seen as a darker contrast than the aqueous regions). Notably, as shown in the inset, 2-3 AuNPs are stacked within the membrane. It has been shown that this particular diblock copolymer, PBD_{35}-*b*-PEO_{20}, yields vesicles with a membrane thickness of 8-10 nm, thus, it is reasonable to observe a stacking of two to three AuNPs with a diameter of 3-5 nm in this region.[1] These images confirm the presence of spherical polymersomes under 200 nm in diameter that contain AuNPs in the hydrophobic region of the membrane.

Conclusion

Both the cryoEM and DLS results collectively indicate that nanovesicles were indeed generated by the method described herein. The final protocol determined by this investigation for the self-assembly of nanovesicles containing AuNPs in the

membrane is as follows: Toluene is evaporated from 20 µl of dodecanethiol-coated AuNPs, and these are then resuspended in 40 µl of THF. A polymer concentration of either 1.5 or 3.0 mM is suitable, depending on desired nanovesicle yield. Finally, Amicon centrifugation filters are used to remove organic solvent and result in AuNP loaded nanovesicles in aqueous suspension.

Developing this protocol was the first step towards "scaling down" this system for applications *in vivo*. Future studies will include determining release dynamics from nanovesicles, which will be challenging without the ability for real-time imaging with fluorescent microscopy. Once release dynamics can be determined and compared to micron-sized vesicles, the nanovesicles can be introduced into mammalian cells (e.g. HeLa cells) and animal systems to determine their applicability as drug carriers *in vivo.*

Concluding Remarks

In this work, polymersomes are generated from PBD_{35}-*b*-PEG_{20} with gold nanoparticles incorporated into the membranes. These AuNP loaded polymersomes are compared to vesicles w/o AuNPs to investigate the effectiveness of the photosensitizer. In all cases, the addition of AuNPs lowers the pulse energy required to induce membrane disruption. It was found that pulse duration influences the amount of energy required to induce complete rupture.

Monitoring the encapsulant release from polymersomes after irradiating at various femtosecond pulse energies demonstrates the ability to tune release, while maintaining the structural integrity of the vesicle. Avoiding the complete disassembly of the vesicle, as in the case with rupture, may be advantageous regarding the clearance of the copolymer/AuNP materials out of the body. Using an analytical model based on diffusion, an effective pore size was determined and shown to increase with increasing pulse energy. Moreover, a critical surface area ratio associated with the poration/rupture boundary was identified and indicates a range for stable pore formation.

There exists a demand for drug delivery systems with high spatial and temporal resolution. The use of plasmonic nanoparticles provides a wavelength-specific, photosensitive system that can potentially be tuned to the NIR, thereby minimizing absorption in the biological window. Applications for this fundamental study include, but are not limited to, precision medicine, nanosurgery and microreactors. Here, a model system on the micron level is investigated to ease

characterization and analysis with optical microscopy. As demonstrated, it is possible to scale down this system to nanovesicles to make it biologically applicable.

Overall, this body of work has demonstrated nanoparticle mediated membrane disruption via single pulse irradiation of PBD_{35}-*b*-PEG_{20} polymersomes and the controlled release of an encapsulant, thereby exhibiting high spatial and temporal resolution.

Appendix I: Table of Abbreviations

ABBREVIATION	DESCRIPTION
a	effective pore radius
AuNP	Gold nanoparticles
cryoEM	cryogenic transmission electro microscopy
D	diffusion coefficient
ddiH20	Deionized distilled water
ddt	dodecanethiol
DLS	Dynamic light scattering
FITC-dextran	Fluorescein isothiocyanate-dextran
fs	femtosecond
IR	infrared
ns	nanosecond
Θ_0	half angle of the cone
PBD-b-PEO	Polybutadiene$_{35}$(1,2 addition)-b-ethyleneoxide$_{20}$
PDMS	Polydimethylsiloxane
psomes	polymersomes
PTFE	Polytetrafluoroethylene
PZn_2	meso-to-meso ethyne-bridged bis[(porphinato)zinc]
R	radius of the polymersome
ROI	region of interest
SEM	standard error of the mean
SPR	Surface plasmon resonance

Abbreviation	Description
t	time elapsed after single pulse
UV	ultraviolet
w/ AuNP	gold nanoparticles in membrane
w/o AuNP	no gold nanoparticles in membrane
τ	Diffusion time

Appendix II: Standard Operating Procedures and Safety of Laser

First, the laser system of choice is powered on and warmed up for thirty minutes, following manufacturer protocols. Small adjustments are made to the internal hardware to maximize the peak power output at 532 nm. With the laser output tuned up, and no objective in place, it is ensured that the beam propagates in an unobstructed manner through the optical path. The energy delivered to the sample is measured with an energy meter placed in the sample holder with the attenuator adjusted to the desired output level. To measure the spot size, the laser should be set to single pulse mode and the desired objective should be in place. The spot size is then measured using a burn spot approach through a dipping objective submerged in water. A Sharpie marker is used to make small dots on the bottom of a glass petri dish, focused in darkfield mode, and a single pulse of irradiation is used to create a defect (burn spot) in the sharpie marker. This process is repeated a minimum of three times and the average spot size is determined by measuring the defect using the Zen software.

At all times, the proper laser safety protocol was strictly adhered to. This includes, but is not limited to, the use of laser goggles and laser curtains at all entrances. An interlocked cover was placed over the eyepiece, as a secondary precaution to physically block the user from accidentally looking into the microscope when the beam path was open to the laser. All users must complete a laser safety training course and be trained on all equipment prior to use.

Appendix III: Additional Information for Chapter 3

Table 1. An example calculation for normalized intensity graphed in Figures 10 and 12

Polymersomes w/ AuNPs in Membrane irradiated at 211.94 nJ. The fluorescence intensity was determined in the selected ROI by the Zeiss software and was corrected by subtracting the intensity in an ROI set in the black background. The ROIs were placed in the same position for every image of the same time series.

TIME (SEC)	INTENSITY	BACKGROUND	CORRECTED INTENSITY	NORMALIZED INTENSITY
0	246.012	99.138	146.874	1.000
3	217.200	98.719	118.481	0.807
13	178.771	100.386	78.385	0.534
23	156.263	99.510	56.753	0.386
33	143.353	99.279	44.074	0.300
43	137.145	98.605	38.540	0.262
53	133.314	98.826	34.488	0.235
63	132.009	99.534	32.475	0.221
73	129.789	98.084	31.705	0.216
83	127.915	98.950	28.965	0.197
93	126.216	98.873	27.343	0.186
103	123.239	97.254	25.985	0.177
113	123.043	97.137	25.906	0.176

Table 2. Values used to calculate a, effective pore radius with error
Radius was measured using Zen software. τ and adjusted R^2 of the fit were calculated using Origin as explained in Chapter 3. Pore radii were calculated using Mathematica. The rows in each data set represent individual vesicles, and the average (gray) is shown in Figure 10 as normalized fluorescence decay.

Energy (nJ)	Radius (μm)	τ	Pore Radius (μm)	Adj. R^2
211.94	21.85	44.35	2.07	0.986
	25.91	47.43	3.23	0.987
	24.40	18.04	7.01	0.997
	19.90	16.04	4.30	0.997
Average	23.02	31.47	4.15	0.992
St. dev.	2.31	14.48	1.83	0.01
175.35	21.05	37.21	2.21	0.999
	23.50	18.14	6.24	0.995
	24.30	12.99	9.54	0.987
	25.65	55.39	2.69	0.989
Average	23.63	30.93	5.17	0.993
St. dev.	1.67	16.76	2.96	0.00
143.04	21.95	34.50	2.70	0.983
	22.85	170.56	0.62	0.991
	29.40	62.00	3.61	0.991
Average	24.73	89.02	2.31	0.988
St. dev.	3.32	58.74	1.25	0.00
110.72	14.45	15.29	1.74	0.932
	23.85	54.37	2.20	0.654
	18.45	8.52	6.39	0.973
Average	18.92	26.06	3.44	0.853
St. dev.	3.85	20.21	2.09	0.14
81.73	23.90	29.15	4.11	0.988
	20.35	28.09	2.64	0.996
	23.05	82.60	1.32	0.948
Average	22.43	46.61	2.69	0.977
St.dev	1.51	25.45	1.14	0.02

Energy (nJ)	Radius (μm)	τ	Pore Radius (μm)	Adj. R^2
63.20	23.90	90.16	1.34	0.996
	24.10	110.67	1.12	0.989
	19.00	36.65	1.65	0.990
	22.35	34.38	2.86	0.988
Average	22.34	67.97	1.74	0.991
St. dev.	2.04	33.26	0.67	0.00
52.27	24.65	-3.68	--	0.974
	24.15	70.88	1.76	0.999
	18.95	33.90	1.77	0.995
	15.10	28.23	1.07	0.977
Average	20.71	32.33	1.53	0.986
St. dev.	3.93	26.47	0.33	0.01
50.85	20.40	29.60	2.52	0.996
	23.45	35.00	3.24	0.864
	26.10	39.72	3.93	0.992
	22.00	28.17	3.32	0.996
Average	22.99	33.12	3.25	0.962
St. dev.	2.10	4.58	0.50	0.06
39.25	23.89	122.43	0.99	0.635
	20.60	204.07	0.38	0.627
	22.88	141.58	0.75	0.849
	17.13	16.35	2.70	0.679
Average	21.13	121.11	1.21	0.698
St. dev.	2.60	67.60	0.89	0.09
32.47	28.98	0.69	--	-0.345
	24.55	63.26	--	0.147
	28.06	43.82	4.43	0.961
Average	27.20	35.92	--	0.254
St. dev.	1.91	26.15	N/A	0.54

References

1. Bermudez, H.; Brannan, A. K.; Hammer, D. A.; Bates, F. S.; Discher, D. E. Molecular Weight Dependence of Polymersome Membrane Structure, Elasticity, and Stability. *Macromolecules* **2002***, 35*, 8203-8208.

2. LoPresti, C.; Lomas, H.; Massignani, M.; Smart, T.; Battaglia, G. Polymersomes: nature inspired nanometer sized compartments. *J. Mater. Chem.* **2009***, 19*, 3576-3590.

3. Haas, S.; Hain, N.; Raoufi, M.; Handschuh-Wang, S.; Wang, T.; Jiang, X.; Schönherr, H. Enzyme Degradable Polymersomes from Hyaluronic Acid-block-poly(ε-caprolactone) Copolymers for the Detection of Enzymes of Pathogenic Bacteria. *Biomacromolecules* **2015***, 16*, 832-841.

4. Egli, S.; Schlaad, H.; Bruns, N.; Meier, W. Functionalization of Block Copolymer Vesicle Surfaces. *Polymers* **2011***, 3*, 252-280.

5. Chen, F.; Qian, J. Studies on the thermal degradation of polybutadiene. *Fuel Process. Technol.* **2000***, 67*, 53-60.

6. Li, W.; Zhan, P.; De Clercq, E.; Lou, H.; Liu, X. Current drug research on PEGylation with small molecular agents. *Prog. Polym. Sci.* **2013***, 38*, 421-444.

7. Lomas, H.; Johnston, A. P. R.; Such, G. K.; Zhu, Z.; Liang, K.; Van Koeverden, M. P.; Alongkornchotikul, S.; Caruso, F. Polymersome-Loaded Capsules for Controlled Release of DNA. *Small* **2011***, 7*, 2109-2119.

8. Yassin, M. A.; Appelhans, D.; Mendes, R. G.; Rümmeli, M. H.; Voit, B. pH-Dependent Release of Doxorubicin from Fast Photo-Cross-Linkable Polymersomes Based on Benzophenone Units. *Chem. Eur. J.* **2012***, 18*, 12227-12231.

9. Kim, H.; Kang, Y. J.; Kang, S.; Kim, K. T. Monosaccharide-Responsive Release of Insulin from Polymersomes of Polyboroxole Block Copolymers at Neutral pH. *J. Am. Chem. Soc.* **2012***, 134*, 4030-4033.

10. Liu, G.; Wang, X.; Hu, J.; Zhang, G.; Liu, S. Self-Immolative Polymersomes for High-Efficiency Triggered Release and Programmed Enzymatic Reactions. *J. Am. Chem. Soc.* **2014***, 136*, 7492-7497.

11. Yu, S.; Azzam, T.; Rouiller, I.; Eisenberg, A. "Breathing" Vesicles. *J. Am. Chem. Soc.* **2009***, 131*, 10557-10566.

12. Wang, L.; Liu, G.; Wang, X.; Hu, J.; Zhang, G.; Liu, S. Acid-Disintegratable Polymersomes of pH-Responsive Amphiphilic Diblock Copolymers for Intracellular Drug Delivery. *Macromolecules* **2015***, 48*, 7562-7272.

13. Qin, S.; Geng, Y.; Discher, D. E.; Yang, S. Temperature-Controlled Assembly and Release from Polymer Vesicles of Poly(ethylene oxide)-block- poly(N-isopropylacrylamide). *Adv. Mater.* **2006***, 18*, 2905-2909.

14. Bixner, O.; Kurzhals, S.; Virk, M.; Reimhult, E. Triggered Release from Thermoresponsive Polymersomes with Superparamagnetic Membranes. *Materials* **2016***, 9*, Article 29.

15. Tong, X.; Wang, G.; Soldera, A.; Zhao, Y. How can azobenzene block copolymer vesicles be dissociated and reformed by light? *J. Phys. Chem. B* **2005***, 109*, 20281-20287.

16. Huang, L.; Yu, C.; Huang, T.; Xu, S.; Bai, Y.; Zhou, Y. Ultrasound-responsive ultrathin multiblock copolyamide vesicles. *Nanoscale* **2016***, 8*, 4922-4926.

17. Olejniczak, J.; Carling, C.; Almutairi, A. Photocontrolled release using one-photon absorption of visible or NIR light. *J. Controlled Release* **2015***, 219*, 18-30.

18. Bashkatov, A. N.; Genina, E. A.; Kochubey, V. I.; Tuchin, V. V. Optical properties of human skin, subcutaneous and mucous tissues in the wavelength range from 400 to 2000 nm. *J. Phys. D-Appl. Phys.* **2005***, 38*, 2543-2555.

19. Liu, G.; Liu, W.; Dong, C. UV- and NIR-responsive polymeric nanomedicines for on-demand drug delivery. *Polym. Chem.* **2013***, 4*, 3431-3443.

20. Rwei, A. Y.; Wang, W.; Kohane, D. S. Photoresponsive nanoparticles for drug delivery. *Nano Today* **2015***, 10*, 451-467.

21. Wang, X.; Hu, J.; Liu, G.; Tian, J.; Wang, H.; Gong, M.; Liu, S. Reversibly Switching Bilayer Permeability and Release Modules of Photochromic Polymersomes Stabilized by Cooperative Noncovalent Interactions. *J. Am. Chem. Soc.* **2015***, 137*, 15262-15275.

22. Robbins, G. P.; Jimbo, M.; Swift, J.; Therien, M. J.; Hammer, D. A.; Dmochowski, I. J. Photoinitiated Destruction of Composite Porphyrin−Protein Polymersomes. *J. Am. Chem. Soc.* **2009***, 131*, 3872-3874.

23. Griepenburg, J. C.; Sood, N.; Vargo, K. B.; Williams, D.; Rawson, J.; Therien, M. J.; Hammer, D. A.; Dmochowski, I. J. Caging metal ions with visible light-responsive nanopolymersomes. *Langmuir* **2015***, 31*, 799-807.

24. Amstad, E.; Kim, S.; Weitz, D. A. Photo- and Thermoresponsive Polymersomes for Triggered Release. *Angew. Chem. Int. Ed.* **2012***, 51*, 12499-12503.

25. Englebienne, P.; Hoonacker, A. V.; Verhas, M. Surface plasmon resonance: principles, methods and applications in biomedical sciences. *Int. J. Spectrosc.* **2003***, 17*, 255-273.

26. Amendola, V.; Meneghetti, M. Size Evaluation of Gold Nanoparticles by UV−vis Spectroscopy. *J. Phys. Chem. C* **2009***, 113*, 4277-4285.

27. Qin, Z.; Bischof, J. C. Thermophysical and biological responses of gold nanoparticle laser heating. *Chem. Soc. Rev.* **2012***, 41*, 1191-1217.

28. Boutopoulos, C.; Hatef, A.; Fortin-Deschênes, M.; Meunier, M. Dynamic imaging of a single gold nanoparticle in liquid irradiated by off-resonance femtosecond laser. *Nanoscale* **2015***, 7*, 11758-11765.

29. Boulais, E.; Lachaine, R.; Hatef, A.; Meunier, M. Plasmonics for pulsed-laser cell nanosurgery: Fundamentals and applications. *J. Photochem. Rev.* **2013***, 17*, 26-49.

30. Hamad, A. H. Effects of Different Laser Pulse Regimes (Nanosecond, Picosecond and Femtosecond) on the Ablation of Materials for Production of Nanoparticles in Liquid Solution. In *High Energy and Short Pulse Lasers*InTech: Rijeka, 2016; pp 11-21.

31. Greene, A. C.; Sasaki, D. Y.; Bachand, G. D. Forming Giant-sized Polymersomes Using Gel-assisted Rehydration. *J. Vis. Exp.* **2016***, 111*, e54051.

32. Metwally, K.; Mensah, S.; Baffou, G. Fluence Threshold for Photothermal Bubble Generation Using Plasmonic Nanoparticles. *J. Phys. Chem. C* **2015***, 119*, 28586-28596.

33. Astarita, G. Phases. In *Thermodynamics: An Advanced Textbook for Chemical Engineers*; Astarita, G., Ed.; Springer US: Boston, MA, 1989; pp 101-129.

34. Kamat, N. P.; Robbins, G. P.; Rawson, J. S.; Therien, M. J.; Dmochowski, I. J.; Hammer, D. A. A Generalized System for Photo-Responsive Membrane Rupture in Polymersomes. *Adv. Funct. Mater.* **2010***, 20*, 2588-2596.

35. Simon, L.; Ospina, J. On the effusion time of drugs from the open pore of a spherical vesicle. *J. Phys. A* **2016***, 451*, 366-372.

36. Levin, Y.; Idiart, M. A.; Arenzon, J. J. Solute diffusion out of a vesicle. *J. Phys. A* **2004***, 344*, 543-546.

37. Singh, R.; Lillard, J. W. Nanoparticle-based targeted drug delivery. *Exp. Mol. Pathol.* **2009***, 86*, 215-223.

38. Discher, B. M.; Won, Y.; Ege, D. S.; Lee, J. C.; Bates, F. S.; Discher, D. E.; Hammer, D. A. Polymersomes: Tough Vesicles Made from Diblock Copolymers. *Science* **1999***, 284*, 1143-1146.

39. Bozzuto, G.; Molinari, A. Liposomes as nanomedical devices. *Int. J. Nanomedicine* **2015***, 10*, 975-999.

40. Nakamura, Y.; Mochida, A.; Choyke, P. L.; Kobayashi, H. Nanodrug Delivery: Is the Enhanced Permeability and Retention Effect Sufficient for Curing Cancer? *Bioconjugate Chem.* **2016***, 27*, 2225-2238.

41. Yildiz, M. E.; Prud'homme, R. K.; Robb, I.; Adamson, D. H. Formation and characterization of polymersomes made by a solvent injection method. *Polym. Adv. Technol.* **2007***, 18*, 427-432.

42. Lorber, B.; Fischer, F.; Bailly, M.; Roy, H.; Kern, D. Protein analysis by dynamic light scattering: methods and techniques for students. *Biochem. Mol. Biol. Educ.* **2012***, 40*, 372-382.

43. Stetefeld, J.; McKenna, S.; Patel, T. Dynamic light scattering: a practical guide and applications in biomedical sciences. *Biophys. Rev.* **2016***, 8*, 409-427.